

Strongly Anisotropic Charge Dynamics in $\text{La}_3\text{Ni}_2\text{O}_7$ with Coherent-to-Incoherent Crossover of Interlayer Charge Dynamics

Bo Su,^{1,†} Chaoxin Huang,^{2,†} Jianzhou Zhao,^{3,†} Mengwu Huo,² Jianlin Luo,¹ Meng Wang,² and Zhi-Guo Chen,^{1,4,*}

¹*Beijing National Laboratory for Condensed Matter Physics,*

Institute of Physics, Chinese Academy of Sciences, Beijing 100190, China

²*Guangdong Provincial Key Laboratory of Magnetoelectric Physics and Devices,*

School of Physics, Sun Yat-Sen University, Guangzhou 510275, China

³*Co-Innovation Center for New Energetic Materials,*

Southwest University of Science and Technology, Mianyang Sichuan 621010, China and

⁴*Songshan Lake Materials Laboratory, Dongguan Guangdong 523808, China*

We report an optical spectroscopy study of the charge-dynamics anisotropy in the $\text{La}_3\text{Ni}_2\text{O}_7$ single crystals with the electric field of the incident light parallel to the crystalline *c*-axis and *ab*-plane, respectively. The evolution of the low-energy part of its *c*-axis optical conductivity spectra ($\sigma_{1c}(\omega)$) from a Drude component to a finite-energy peak, together with the change in the *c*-axis electron mean-free-path which is distinctly longer than the *c*-axis lattice constant at 10 K but is shorter than the *c*-axis lattice constant at 300 K, demonstrates a crossover from coherent to incoherent interlayer charge dynamics in $\text{La}_3\text{Ni}_2\text{O}_7$, which is associated with the variation from weak to strong dissipation within its *ab*-plane. In contrast, the Drude component robust in its $\sigma_{1ab}(\omega)$ and the long *ab*-plane electron mean-free-path greater than the *a*-axis and *b*-axis unit-cell lengths manifest the persistence of coherent in-plane charge dynamics from 10 to 300 K. Thus, the charge dynamics in $\text{La}_3\text{Ni}_2\text{O}_7$ shows a remarkable anisotropy at *high* temperatures. At *low* temperatures, the large values of the ratio between the *ab*-plane and *c*-axis Drude weights and the ratio $\sigma_{1ab}(\omega \rightarrow 0)/\sigma_{1c}(\omega \rightarrow 0)$ indicate a strong anisotropy of the *low*-temperature charge dynamics in $\text{La}_3\text{Ni}_2\text{O}_7$.

The discovery of superconductivity in the Ruddlesden-Popper double-layered perovskite nickelate $\text{La}_3\text{Ni}_2\text{O}_7$ under high pressure, which exhibits the maximal superconducting transition temperature $T_c \sim 80$ K [1–4], has generated enormous interest in the scientific community [5–35]. Considering that (i) the double-layered perovskite nickelate $\text{La}_3\text{Ni}_2\text{O}_7$, which crystallizes into an orthorhombic phase with a corner-connected NiO_6 octahedral layer separated by a La–O layer along the *c*-axis at ambient pressure (see the schematic of the crystal structure in the inset of Fig. 1(a)) and still hosts the layered crystal structure at high pressures although a structure phase transition occurs at pressures above 10 GPa [1, 35–41], and (ii) the crystal structures of solids are intimately associated with the electronic properties, studying the discrepancy between the *ab*-plane and *c*-axis electronic properties of $\text{La}_3\text{Ni}_2\text{O}_7$ is crucial for developing the theory of anisotropic superconductivity in this double-layered perovskite nickelate [7, 42–69]. However, the anisotropy of the electronic properties in $\text{La}_3\text{Ni}_2\text{O}_7$ has so far been little investigated by experiments.

Charge dynamics is one of fundamental electronic properties, so studying the anisotropy of the charge dynamics in $\text{La}_3\text{Ni}_2\text{O}_7$ is an effective approach for gain insight into its electronic anisotropy [66, 67, 70–80]. For some layered materials, remarkable difference exists between the in-plane and interlayer charge dynamics, e.g., a few underdoped copper oxides and $\text{FeTe}_{0.55}\text{Se}_{0.45}$ show coherent in-plane charge dynamics but incoherent interlayer charge dynamics [72–74]. On the contrary, both in-plane and interlayer charge dynamics are coherent in some other layered materials, such as the undoped iron

pniictides BaFe_2As_2 , the optimally doped iron pniictides $\text{Ba}(\text{Fe}_{0.926}\text{Co}_{0.074})_2\text{As}_2$, $\text{Ba}_{0.67}\text{K}_{0.33}\text{Fe}_2\text{As}_2$ and the optimally doped or overdoped cuprates [73–77]. Therefore, a natural and important question arises as to what degree of the charge-dynamics anisotropy is in $\text{La}_3\text{Ni}_2\text{O}_7$, which is expected to provide an essential boundary for understanding the superconducting anisotropy in this double-layered perovskite nickelate [72–80]. However, as one of the prerequisites for obtaining the degree of the charge-dynamics anisotropy, the interlayer charge dynamics in $\text{La}_3\text{Ni}_2\text{O}_7$ remains elusive.

In underdoped $\text{YBa}_2\text{Cu}_3\text{O}_y$, $\text{YBa}_2\text{Cu}_4\text{O}_8$ and overdoped $\text{Bi}_2\text{Sr}_2\text{CaCu}_2\text{O}_{8+\delta}$, a crossover from incoherent to coherent interlayer charge dynamics were observed as the temperature decreases [67, 68, 81, 82]. The observed incoherent-to-coherent crossover of the interlayer charge dynamics guarantees the three-dimensional metallic states at low temperatures, which was proposed to be significant for the superconducting pair tunnelling along the crystalline *c*-axis and the emergence of the high- T_c superconductivity in the copper oxides [66–69, 83, 84]. Nonetheless, the temperature evolution of the interlayer charge dynamics in $\text{La}_3\text{Ni}_2\text{O}_7$ which has a similar crystal structure with the copper oxides has so far been little investigated by experiments.

Optical spectroscopy is an efficient experimental technique for studying charge-dynamics anisotropy of a material as it can probe itinerant charge carriers using linearly polarized incident light [70–80, 85–89]. Here, to study the charge-dynamics anisotropy in $\text{La}_3\text{Ni}_2\text{O}_7$, we measured the optical reflectance spectra (i.e., $R(\omega)$) of its single crystals at ambient pressure at low temperatures

over a broad photon-energy (ω) range with the light electric field $\mathbf{E} \parallel ab$ -plane and $\mathbf{E} \parallel c$ -axis, respectively (see the details about the reflectance measurements, the sample preparation and the characterizations of the two measured crystal faces which are parallel to the ab -plane and c -axis, respectively in Supplemental Material). The real part ($\sigma_1(\omega)$) of the optical conductivity is obtained via the Kramers-Kronig transformation of the $R(\omega)$. Figure 1(a) depicts the c -axis reflectance spectra $R_c(\omega)$ of $\text{La}_3\text{Ni}_2\text{O}_7$ in the photon-energy range up to 200 meV at different temperatures (see the schematic of the crystal structure in the inset of Fig. 1(a)). Several peak- and dip-like sharp features present in the energy range from 14 to 75 meV in the $R_c(\omega)$ correspond to the spike-like features in the $\sigma_1c(\omega)$ (see Fig. 1(b)), which are assigned as the phonon modes (see the calculated phonon modes in Table S1 and the related calculation details in Supplemental Material). To clearly show the low-energy optical response of electrons, we plotted the $R_c(\omega)$ and the $\sigma_1c(\omega)$ in the energy range up to 17 meV in Fig. 1(c) and 1(d), respectively. Noteworthily, in Fig. 1(d), the $\sigma_1c(\omega)$ at 10 K, 50 K and 100 K exhibit the Drude components—upturn-like features arising from the optical response of the itinerant charge carriers at energies lower than 14 meV, which qualitatively indicate that interlayer charge dynamics in $\text{La}_3\text{Ni}_2\text{O}_7$ is coherent at 10 K, 50 K and 100 K. As the temperature rises, the upturn-like features at 10 K, 50 K and 100 K evolves into the obvious peak-like features centered at finite energies in the low-energy part of the $\sigma_1c(\omega)$ at 150 K, 200 K and 300 K

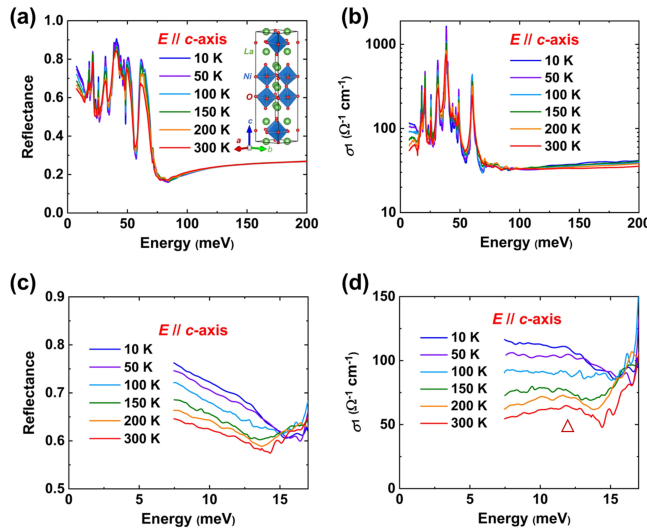


FIG. 1. C -axis optical response of $\text{La}_3\text{Ni}_2\text{O}_7$. (a) c -axis reflectance $R_c(\omega)$ below 200 meV. The inset indicates the crystal structure of $\text{La}_3\text{Ni}_2\text{O}_7$ at ambient pressure. (b) c -axis optical conductivity $\sigma_1c(\omega)$ below 200 meV. (c) $R_c(\omega)$ up to 17 meV. (d) $\sigma_1c(\omega)$ up to 17 meV. The red triangle indicates the finite-energy peak in the low-energy part of the $\sigma_1c(\omega)$ at high temperatures.

(see Fig. 1(d)). The finite-energy peak in the low-energy part of the $\sigma_1c(\omega)$ at high temperatures can serve as a spectroscopic signature of incoherent interlayer charge dynamics in $\text{La}_3\text{Ni}_2\text{O}_7$. Thus, the evolution from the low-temperature Drude feature to the high-temperature finite-energy peak in the low-energy part of the $\sigma_1c(\omega)$ here, which was similarly observed in the copper oxides $\text{La}_{2-x}\text{Sr}_x\text{CuO}_4$ and $\text{Bi}_2\text{Sr}_2\text{CuO}_6$ [89, 90], suggests that as the temperature increases, a crossover from coherent to incoherent interlayer charge dynamics occurs in $\text{La}_3\text{Ni}_2\text{O}_7$.

To quantitatively check the temperature-induced crossover from coherent to incoherent interlayer charge dynamics in $\text{La}_3\text{Ni}_2\text{O}_7$, we need to compare the electron mean free path (l_c) along the c -axis with its c -axis lattice constant (d_c) according to the Mott-Ioffe-Regel criterion [91–93]. In principle, the c -axis mean free path l_c can be estimated via the following relationship:

$$l_c = v_F^Z \tau_c, \quad (1)$$

where v_F^Z is the component of the Fermi velocity along k_z direction, and τ_c is the relaxation time along the c -axis. To obtain the c -axis relaxation time τ_c , we fit the $\sigma_1c(\omega)$ at different temperatures using a standard Drude-Lorentz model (see the fitting parameters in Table S2-7, the Drude and Lorentzian components in Fig. S3 of Supplemental Material) [70, 71]. Figure 2(a) and 2(b) present the Drude-Lorentz fits to the $\sigma_1c(\omega)$ at two typical temperatures 10 K and 300 K, respectively (see the gray fitting curves and the Drude components shaded in violet color). In Fig. 2(c), the scattering rate (i.e., τ_c^{-1}) of the itinerant charge carriers along the c -axis, which is equal to the half-height width of the Drude component, decreases from (96.8 ± 10) to (36.6 ± 3) meV as the temperature is lowered from 300 to 10 K. Correspondingly, the τ_c increases from $(4.3 \pm 0.4) \times 10^{-14}$ s to $(1.1 \pm 0.1) \times 10^{-13}$ s with decreasing temperature from 300 to 10 K. To evaluate the c -axis component of the Fermi velocity, we performed *ab initio* calculations of the Fermi surfaces (FSs) based on the optimized cell geometry at ambient pressure (see the details about *ab initio* calculations in Supplemental Material) [1]. In Fig. 2(d), not only the calculated FSs around the M point, the X point and the Y point but also the calculated FSs around the Γ point along the $X - \Gamma - X$ direction and the $Y - \Gamma - Y$ direction host near-zero v_F^Z , while the calculated FSs around the Γ point along the $M - \Gamma - M$ direction has a nonnegligible component of the Fermi velocity along k_z -direction $v_{F(DFT)}^Z = 6.71 \times 10^4$ m/s. Noteworthily, compared with the measured electronic bands, the electronic bands obtained by *ab initio* calculations host the reduced Fermi velocities due to orbital-dependent electronic correlations [43, 44, 54, 55, 58, 61]. Considering the renormalization factor (~ 1.8) for the electronic band generating the FS around the Γ point along the $M - \Gamma - M$ direction [43], the k_z -direction component of the renormalized Fermi veloc-

ity on the FS around the Γ point along the $M - \Gamma - M$ direction $v_{F(REN)}^Z = v_{F(DFT)}^Z / 1.8 \approx 3.72 \times 10^4$ m/s. Thus, according to Eq. (1), the l_c at 10 K and 300 K can be estimated to be $\sim (42.1 \pm 4)$ Å and $\sim (15.9 \pm 2)$ Å, respectively. Therein, the l_c at 10 K are distinctly longer than the d_c of $\text{La}_3\text{Ni}_2\text{O}_7$, which quantitatively demonstrates the coherent interlayer charge dynamics in $\text{La}_3\text{Ni}_2\text{O}_7$ at 10 K. By contrast, the l_c at 300 K is a little bit shorter than the d_c , which quantitatively confirms the incoherent interlayer charge dynamics in $\text{La}_3\text{Ni}_2\text{O}_7$ at 300 K. Figure 2(e) shows that the l_c at $T < 150$ K is remarkably longer than the d_c , while the l_c at $T \geq 150$ K is shorter than the d_c , which further verifies the temperature-induced crossover from coherent to incoherent interlayer charge dynamics in $\text{La}_3\text{Ni}_2\text{O}_7$.

Previous investigations suggest that the c -axis charge dynamics in a large number of layered materials including the copper oxides, the iron pnictide BaFe_2As_2 and the iron chalcogenide $\text{FeTe}_{0.55}\text{Se}_{0.45}$ may be associated with the dissipation within the ab -plane [72, 74, 86, 94]. To study whether the temperature-induced crossover from coherent to incoherent interlayer charge dynamics in $\text{La}_3\text{Ni}_2\text{O}_7$ is related to the change in the dissipation

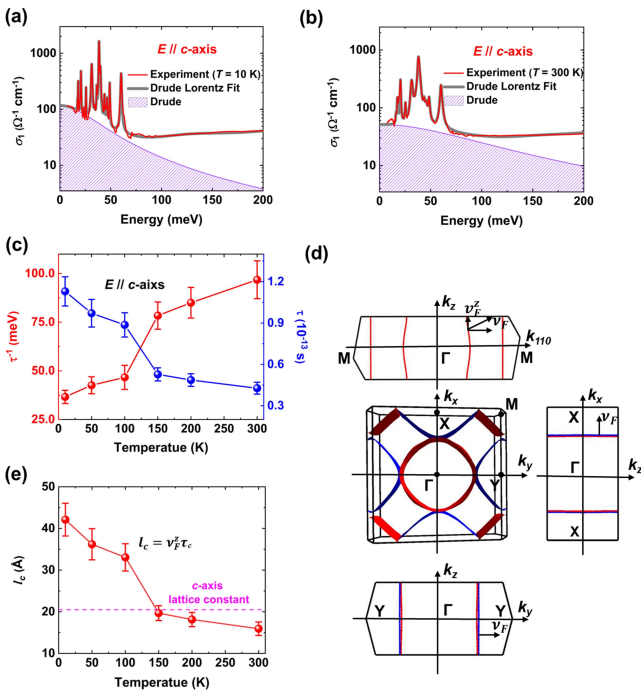


FIG. 2. Estimation of the c -axis mean free path l_c . (a) and (b) Drude components in the $\sigma_{1c}(\omega)$ at 10 K and 300 K. (c) Temperature evolutions of the c -axis scattering rate τ_c^{-1} and relaxation time τ_c . (d) Calculated FSs of $\text{La}_3\text{Ni}_2\text{O}_7$ at ambient pressure in three-dimensional (3D) Brillouin zone and the side views of the FSs along the $M - \Gamma - M$ direction, the $X - \Gamma - X$ direction and the $Y - \Gamma - Y$ direction. (e) Estimated l_c as a function of temperature. The pink dashed line indicates the c -axis lattice constant.

within the ab -plane, we measured its ab -plane reflectance spectra $R_{ab}(\omega)$. Figure 3(a) depicts the measured $R_{ab}(\omega)$ and $\sigma_{1ab}(\omega)$ of the $\text{La}_3\text{Ni}_2\text{O}_7$ single crystals at two representative temperatures 10 K and 300 K in the energy range up to 200 meV (see the $R_{ab}(\omega)$ and $\sigma_{1ab}(\omega)$ at the other temperatures in Fig. S4 of Supplemental Material). At energies lower than 50 meV, the $R_{ab}(\omega)$ at 10 K not only is higher than that at 300 K but also approaches to unity, which shows the metal-like optical response. Correspondingly, in Fig. 3(a), the $\sigma_{1ab}(\omega)$ at 10 K and 300 K exhibit the Drude components at low energies. To get access to the ab -plane charge dynamics in $\text{La}_3\text{Ni}_2\text{O}_7$, we fit the $\sigma_{1ab}(\omega)$ at 10 K and 300 K based on the standard Drude-Lorentz model (see the fitting parameters in Table S2-7, the Drude and Lorentzian components in Fig. S5 of Supplementary Material). Figure 3(b) and 3(c) display the Drude-Lorentz fits to the $\sigma_{1ab}(\omega)$ at 10 K and 300 K, respectively (see the gray fitting curves and the Drude components shaded in violet color). The ab -plane Drude weight S_{ab} obtained by the Drude-Lorentz fits were plotted as a function of temperature in Fig. 3(d). Since previous theoretical analysis and ab *initio* calculations suggest that at ambient pressure, the electronic bands of $\text{La}_3\text{Ni}_2\text{O}_7$ crossing the Fermi energy are dominated by the single $3d_{x^2-y^2}$ orbital [1, 11, 35, 43, 53], the extended Drude model involving the S_{ab} , which works under the assumption of a single-band response, was employed to obtain the ab -plane scattering rate spectra $\tau_{ab}(\omega)$ of $\text{La}_3\text{Ni}_2\text{O}_7$. Figure 3(e) shows that in the energy region ($\omega < 40$ meV) of the Drude response at 10 K, the $\tau_{ab}(\omega)$ at 10 K is in the Landau-Fermi-liquid region, i.e., $\tau_{ab}(\omega < 40 \text{ meV}, T = 10 \text{ K}) < \omega$, which suggests weak dissipation within the ab -plane at 10 K. Similar to the cases in a large variety of layered materials, the weak dissipation within the ab -plane of $\text{La}_3\text{Ni}_2\text{O}_7$ is likely to correspond to the existence of well-defined quasi-particles and is associated with its coherent c -axis charge dynamics. On the contrary, the $\tau_{ab}(\omega < 40 \text{ meV})$ at 300 K is beyond the Landau-Fermi-liquid region, i.e., $\tau_{ab}(\omega < 40 \text{ meV}, T = 300 \text{ K}) > \omega$, which suggests strong dissipation within the ab -plane at 300 K and is consistent with the incoherent c -axis charge dynamics revealed by the finite-energy peak in the low-energy part of the $\sigma_{1c}(\omega)$ and the estimated l_c shorter than the d_c . Thus, our results show that the temperature-induced crossover from coherent to incoherent interlayer charge dynamics in $\text{La}_3\text{Ni}_2\text{O}_7$ correlates to the variation in the dissipation within the ab -plane.

Before studying the degree of the charge-dynamic anisotropy in $\text{La}_3\text{Ni}_2\text{O}_7$, it is essential to gain insight into the nature of its ab -plane charge dynamics in the temperature range from 300 to 10 K. In Fig. 3(f), the ab -plane scattering rate at 10 K and 300 K, which were obtained by the Drude-Lorentz fits to the $\sigma_{1ab}(\omega)$, correspond to the ab -plane-relaxation times $\tau_{ab}(10 \text{ K}) = (6.4 \pm 1.3) \times 10^{-13} \text{ s}$ and $\tau_{ab}(300 \text{ K}) = (9.8 \pm 1.6) \times 10^{-14} \text{ s}$. More-

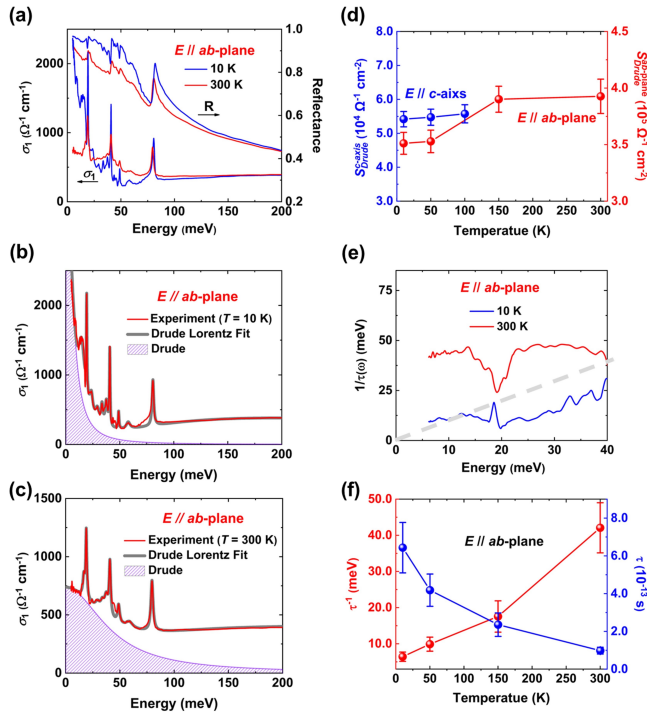


FIG. 3. *Ab*-plane optical response of $\text{La}_3\text{Ni}_2\text{O}_7$. (a) *ab*-plane reflectance $R_{ab}(\omega)$ and optical conductivity $\sigma_{1ab}(\omega)$ at 10 K and 300 K in the energy range up to 200 meV. (b) and (c) Drude components in the $\sigma_{1ab}(\omega)$ at 10 K and 300 K. (d) *ab*-plane and *c*-axis Drude weights (S_{ab} and S_c) at different temperatures. (e) *ab*-plane scattering rate spectra $1/\tau_{ab}(\omega)$ at 10 K and 300 K. The dashed line represents the relationship $1/\tau_{ab}(\omega) = \omega$. (f) *ab*-plane scattering rate τ_{ab}^{-1} and relaxation time τ_{ab} at different temperatures.

over, *ab initio* calculations reveal that the FSs around the Γ point along the $M - \Gamma - M$ direction, the FSs around the M point along the $M - \Gamma - M$ direction, and the FSs around the X (or Y) point along the $X - \Gamma - X$ (or $Y - \Gamma - Y$) direction host the components of the Fermi velocities parallel to the k_x - k_y plane $v_F^{xy(DFT)} \approx 4.70 \times 10^5$ m/s, 5.00×10^5 m/s and 6.06×10^5 m/s, respectively (see Fig. 2(d)). Considering that the renormalization factors (i.e., 1.8, 2.6 and 2.3) for the corresponding electronic bands [43], the experimental k_x - k_y -plane components of the renormalized Fermi velocities on the FSs around the Γ point along the $M - \Gamma - M$ direction, on the FSs around the M point along the $M - \Gamma - M$ direction, and on the FSs around the X (or Y) point along the $X - \Gamma - X$ (or $Y - \Gamma - Y$) direction $v_F^{xy(REN)} \approx 2.61 \times 10^5$ m/s, 1.92×10^5 m/s and 2.63×10^5 m/s, respectively. Given the relationship among the *ab*-plane mean free paths l_{ab} , the component of the Fermi velocities parallel to the k_x - k_y plane v_F^{xy} and τ_{ab} :

$$l_{ab} = v_F^{xy} \tau_{ab}, \quad (2)$$

for the charge carriers on the FSs around the Γ point along the $M - \Gamma - M$ direction, on the FSs around the

M point along the $M - \Gamma - M$ direction, and on the FSs around the X (or Y) point along the $X - \Gamma - X$ (or $Y - \Gamma - Y$) direction, the $l_{ab}(300 \text{ K}) \approx (256.6 \pm 40) \text{ \AA}$, $(189.1 \pm 30) \text{ \AA}$ and $(258.9 \pm 40) \text{ \AA}$, respectively (see Fig. 4(a)). As the temperature is lowered down to 10 K, the l_{ab} increase to $\sim (1679.4 \pm 350) \text{ \AA}$, $\sim (1237.6 \pm 260) \text{ \AA}$ and $\sim (1694.6 \pm 350) \text{ \AA}$, respectively (see Fig. 4(a)). Thus, in the temperature range 300–10 K, all the estimated l_{ab} are much longer than the unit cell lengths of $\text{La}_3\text{Ni}_2\text{O}_7$ along the *a*-axis and *b*-axis, i.e., $d_a \sim 5.40 \text{ \AA}$ and $d_b \sim 5.43 \text{ \AA}$. According to the Mott-Ioffe-Regel criterion, the *ab*-plane charge dynamics in $\text{La}_3\text{Ni}_2\text{O}_7$ should be coherent from 300 to 10 K, which is quite different from its incoherence interlayer charge dynamics at high temperatures. Thus, $\text{La}_3\text{Ni}_2\text{O}_7$ exhibits strongly anisotropic charge dynamics at *high* temperatures.

To qualitatively study the charge-dynamic anisotropy in $\text{La}_3\text{Ni}_2\text{O}_7$ at *low* temperature, we plotted the $R_{ab}(\omega)$ and $R_c(\omega)$ at 10 K over a broad energy range up to 200 meV in Fig. 4(b). Compared with the $R_c(\omega)$, the $R_{ab}(\omega)$ exhibits a very different photon-energy dependence. Correspondingly, Fig. 4(c) shows that the low-energy part ($\omega < 50$ meV) of the $\sigma_{1ab}(\omega)$ at 10 K, which includes the Drude component, is much higher than that of the $\sigma_{1c}(\omega)$ at 10 K. The great discrepancy between the low-energy part of the $\sigma_{1ab}(\omega)$ and the $\sigma_{1c}(\omega)$ of $\text{La}_3\text{Ni}_2\text{O}_7$ at 10 K, which reflects the 2D-like FSs, suggests that the anisotropy of its charge dynamics should be also strong at *low* temperatures. Moreover, in Fig. 2(d), our *ab initio* calculations show that the k_z components of all the Fermi velocities normal to the FSs are much smaller than the components of the Fermi velocities parallel to the k_x - k_y plane, which indicates two-dimensional (2D) like FSs and further supports the strongly anisotropic charge dynamics in $\text{La}_3\text{Ni}_2\text{O}_7$ at *low* temperatures.

To quantitatively study the degree of the charge-dynamics anisotropy in $\text{La}_3\text{Ni}_2\text{O}_7$ at *low* temperatures, we plotted the $\sigma_{1ab}(\omega \rightarrow 0)$ and the $\sigma_{1c}(\omega \rightarrow 0)$ at different temperatures in Fig. 4(d), which were obtained by the Hagen-Rubens low-energy extrapolation of the $R_{ab}(\omega)$ and $R_c(\omega)$, respectively (see the Method, Fig. S2 and Fig. S4 in Supplemental Material). At 10 K, the ratio $\sigma_{1ab}(\omega \rightarrow 0)/\sigma_{1c}(\omega \rightarrow 0)$ of $\text{La}_3\text{Ni}_2\text{O}_7$ shows the value of ~ 36 , which is higher than $\sigma_{1ab}(\omega \rightarrow 0)/\sigma_{1c}(\omega \rightarrow 0)$ of the “122” type iron-pnictide superconductors BaFe_2As_2 (~ 1.6) [75, 95], optimally doped $\text{Ba}_{1-x}\text{K}_x\text{Fe}_2\text{As}_2$ (~ 3.1) and $\text{Ba}(\text{Fe}_{1-x}\text{Co}_x)_2\text{As}_2$ (~ 3.4) [76, 77], but is significantly less than the $\sigma_{1ab}(\omega \rightarrow 0)/\sigma_{1c}(\omega \rightarrow 0)$ of the fully oxygenated copper-oxide superconductor $\text{YBa}_2\text{Cu}_3\text{O}_{7-\delta}$ (~ 40) and overdoped copper-oxide superconductor $\text{La}_{2-x}\text{Sr}_x\text{CuO}_4$ (~ 113) (see Fig. 4(e)) [73, 74, 96, 97]. Moreover, according to the S_{ab} and S_c of $\text{La}_3\text{Ni}_2\text{O}_7$ in Fig. 3(d), we can get the ratio $S_{ab}/S_c \sim 6.5$ at 10 K, which is larger than the S_{ab}/S_c of the “122” type iron-pnictide superconductors BaFe_2As_2 (~ 1.7) [75], optimally doped $\text{Ba}_{1-x}\text{K}_x\text{Fe}_2\text{As}_2$

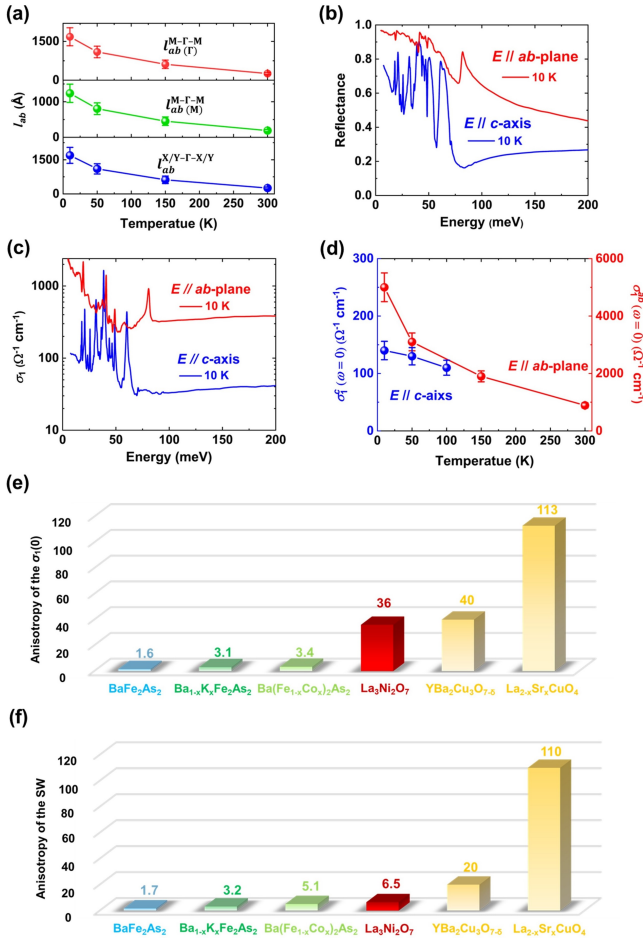


FIG. 4. Strongly anisotropic charge dynamics. (a) ab -plane mean free paths l_{ab} for the charge carriers on the FSs around the Γ point along the $M - \Gamma - M$ direction (see the red dots), on the FSs around the M point along the $M - \Gamma - M$ direction (see the green dots) and on the FSs around the X (or Y) point along the $X - \Gamma - X$ (or $Y - \Gamma - Y$) direction (see the blue dots). (b) $R_{ab}(\omega)$ and $R_c(\omega)$ at 10 K. (c) $\sigma_{1ab}(\omega)$ and $\sigma_{1c}(\omega)$ at 10 K. (d) $\sigma_{1ab}(\omega \rightarrow 0)$ and $\sigma_{1c}(\omega \rightarrow 0)$ obtained by the Hagen-Rubens low-energy extrapolations. (e) Ratios $\sigma_{1ab}(\omega \rightarrow 0)/\sigma_{1c}(\omega \rightarrow 0)$ of La₃Ni₂O₇, the iron-pnictide superconductors and the copper-oxide superconductors at low temperatures [73–77, 95–97]. (f) Ratios S_{ab}/S_c of La₃Ni₂O₇, the iron-pnictide superconductors and the copper-oxide superconductors at low temperatures [73, 75–77, 96].

(~ 3.2) and Ba(Fe_{1-x}Co_x)₂As₂ (~ 5.1) [76, 77], but is much smaller than the S_{ab}/S_c of the fully oxygenated copper-oxide superconductor YBa₂Cu₃O_{7-δ} (~ 20) and overdoped copper-oxide superconductor La_{2-x}Sr_xCuO₄ (~ 110) (see Fig. 4(f)) [73, 96]. Thus, the large values of the ratios S_{ab}/S_c and $\sigma_{1ab}(\omega \rightarrow 0)/\sigma_{1c}(\omega \rightarrow 0)$ in La₃Ni₂O₇ at 10 K indicate that its low-temperature charge dynamics exhibits a strong anisotropy with its degree located between the “122” type iron-pnictide superconductors and the fully oxygenated/overdoped copper-oxide superconductors. Noteworthily, the “122” type

iron-pnictide superconductors host the large-size 3D ellipsoid FS with the dominant Fe-3d_{3z²-r²} orbital enclosing the Z point of the Brillouin zone and the quasi-2D cylinder-like FSs with small warping along k_z around the Γ point and the corners of the Brillouin zone [75, 98–100], while in La₃Ni₂O₇, except that the FS around the Γ point along the $M - \Gamma - M$ direction has a small Fermi-velocity component along k_z direction, the majority of the FSs are quasi-2D and have the Fermi velocities substantially parallel to the k_x - k_y plane (see Fig. 2(d)), which supports that La₃Ni₂O₇ exhibits a stronger anisotropy of charge dynamics than the “122” type iron-pnictide superconductors. Moreover, although both the copper oxides and La₃Ni₂O₇ have quasi-2D FSs dominated by 3d_{x²-y²} orbitals [1, 7, 25, 35, 101], a theoretical study indicates that the interlayer hopping term related to the Ni 3d_{x²-y²} orbital in La₃Ni₂O₇ is remarkably larger than that associated with the Cu 3d_{x²-y²} orbital in the copper oxides [7, 53], which also suggests that the charge-dynamics anisotropy in La₃Ni₂O₇ is weaker than those in the copper oxides.

In summary, we have investigated the interlayer charge dynamics and the charge-dynamics anisotropy in La₃Ni₂O₇. Considering that (i) as the temperature increases, the Drude component in the low-energy region of the $\sigma_{1c}(\omega)$ evolves into a finite-energy peak, and (ii) at 10 K, $l_c > d_c$ but at 300 K, $l_c < d_c$, a crossover from coherent to incoherent interlayer charge dynamics occurs in La₃Ni₂O₇, which is related to the variation from weak to strong dissipation within its ab -plane. By contrast, in the temperature range 10–300 K, the robustness of the Drude component in its $\sigma_{1ab}(\omega)$, together with $l_{ab} \gg d_a$ and $l_{ab} \gg d_b$, demonstrates that the in-plane charge dynamics is coherent. Thus, the anisotropy of the charge dynamics in La₃Ni₂O₇ is remarkable at high temperatures. At low temperatures, the large values of the ratios S_{ab}/S_c and $\sigma_{1ab}(\omega \rightarrow 0)/\sigma_{1c}(\omega \rightarrow 0)$ indicate that the anisotropy of the low-temperature charge dynamics is strong in La₃Ni₂O₇.

We thanks Prof. Tao Xiang for very helpful and fruitful discussions. The authors acknowledge support from the strategic Priority Research Program of Chinese Academy of Sciences (Project No. XDB33000000), the National Natural Science Foundation of China (Grant No. U21A20432 and 12174454), the National Key Research and Development Program of China (Grant No. 2022YFA1403800 and 2023YFA1406500), the Guangdong Basic and Applied Basic Research Foundation (Projects No. 2021B1515130007 and 2024B1515020040), Guangzhou Basic and Applied Basic Research Funds (Grant No. 2024A04J6417), and Guangdong Provincial Key Laboratory of Magnetoelectric Physics and Devices (Grant No. 2022B1212010008) and the Synergetic Extreme Condition User Facility (SECUF) Infrared Unit in THz and Infrared Experimental Station. Z.-G.C. conceived and supervised this project. C.H., M.H., and

M.W. grew the single crystals. C.H., M.H. and B.S. performed the characterization of the single crystals. B.S. carried out the optical experiments. J.Z. did first-principle calculations. Z-G.C., B.S., J.Z. and J.L. analyzed the data. Z-G.C. and B.S. wrote the paper.

[†]B. S., J.Z. and C. H. contributed equally to this work.

* zgchen@iphy.ac.cn

- [1] H. Sun, M. Huo, X. Hu, J. Li, Z. Liu, Y. Han, L. Tang, Z. Mao, P. Yang, B. Wang, J. Cheng, D.-X. Yao, G.-M. Zhang, and M. Wang, *Nature* **621**, 493 (2023).
- [2] Y. Zhang, D. Su, Y. Huang, Z. Shan, H. Sun, M. Huo, K. Ye, J. Zhang, Z. Yang, Y. Xu, Y. Su, R. Li, M. Smidman, M. Wang, L. Jiao, and H. Yuan, *Nat. Phys.* **20**, 1269 (2024).
- [3] J. Hou, P.-T. Yang, Z.-Y. Liu, J.-Y. Li, P.-F. Shan, L. Ma, G. Wang, N.-N. Wang, H.-Z. Guo, J.-P. Y. U. Sun, M. Wang, G.-M. Zhang, B.-S. Wang, and J.-G. Cheng, *Chinese Phys. Lett.* **40**, 117302 (2023).
- [4] G. Wang, N. Wang, X. Shen, J. Hou, L. Ma, L. Shi, Z. Ren, Y. Gu, H. Ma, P. Yang, Z. Liu, H. Guo, J. Sun, G. Zhang, S. Calder, J.-Q. Yan, B. Wang, Y. Uwatoko, and J.-G. Cheng, *Phys. Rev. X* **14**, 011040 (2024).
- [5] Z. Liu, M. Huo, J. Li, Q. Li, Y. Liu, Y. Dai, X. Zhou, J. Hao, Y. Lu, M. Wang, and H.-H. Wen, *Nat. Commun.* **15**, 7570 (2024).
- [6] X. Chen, P. Jiang, J. Li, Z. Zhong, and Y. Lu, “Critical charge and spin instabilities in superconducting $\text{La}_3\text{Ni}_2\text{O}_7$ ” (2024), arXiv:2307.07154.
- [7] Z. Fan, J.-F. Zhang, B. Zhan, D. Lv, X.-Y. Jiang, B. Normand, and T. Xiang, *Phys. Rev. B* **110**, 024514 (2024).
- [8] Z. Dong, M. Huo, J. Li, J. Li, P. Li, H. Sun, L. Gu, Y. Lu, M. Wang, Y. Wang, and Z. Chen, *Nature* **630**, 847 (2024).
- [9] M. Wang, H.-H. Wen, T. Wu, D.-X. Yao, and T. Xiang, *Chinese Phys. Lett.* **41**, 077402 (2024).
- [10] Q. Qin and Y.-f. Yang, *Phys. Rev. B* **108**, L140504 (2023).
- [11] Q.-G. Yang, D. Wang, and Q.-H. Wang, *Phys. Rev. B* **108**, L140505 (2023).
- [12] J. Huang, Z. D. Wang, and T. Zhou, *Phys. Rev. B* **108**, 174501 (2023).
- [13] Y.-B. Liu, J.-W. Mei, F. Ye, W.-Q. Chen, and F. Yang, *Phys. Rev. Lett.* **131**, 236002 (2023).
- [14] K. Jiang, Z. Wang, and F.-C. Zhang, *Chinese Phys. Lett.* **41**, 017402 (2024).
- [15] H. Lange, L. Homeier, E. Demler, U. Schollwöck, F. Grusdt, and A. Bohrdt, *Phys. Rev. B* **109**, 045127 (2024).
- [16] X.-Z. Qu, D.-W. Qu, J. Chen, C. Wu, F. Yang, W. Li, and G. Su, *Phys. Rev. Lett.* **132**, 036502 (2024).
- [17] X. Chen, J. Zhang, A. S. Thind, S. Sharma, H. LaBolita, G. Peterson, H. Zheng, D. P. Phelan, A. S. Botana, R. F. Klie, and J. F. Mitchell, *J. Am. Chem. Soc.* **146**, 3640 (2024).
- [18] R. Gao, L. Jin, S. Huyan, D. Ni, H. Wang, X. Xu, S. L. Bud'ko, P. Canfield, W. Xie, and R. J. Cava, *ACS Appl. Mater. Interfaces.* (2024).
- [19] Z. Dan, Y. Zhou, M. Huo, Y. Wang, L. Nie, M. Wang, T. Wu, and X. Chen, “Spin-density-wave transition in double-layer nickelate $\text{La}_3\text{Ni}_2\text{O}_7$ ” (2024), arXiv:2402.03952.
- [20] S. N. Abadi, K.-J. Xu, E. G. Lomeli, P. Puphal, M. Isobe, Y. Zhong, A. V. Fedorov, S.-K. Mo, M. Hashimoto, D.-H. Lu, B. Moritz, B. Keimer, T. P. Devereaux, M. Hepting, and Z.-X. Shen, “Electronic structure of the alternating monolayer-trilayer phase of $\text{La}_3\text{Ni}_2\text{O}_7$ ” (2024), arXiv:2402.07143.
- [21] R. Khasanov, T. J. Hicken, D. J. Gawryluk, L. P. Sorel, S. Böttzel, F. Lechermann, I. M. Eremin, H. Luetkens, and Z. Guguchia, “Pressure-induced split of the density wave transitions in $\text{La}_3\text{Ni}_2\text{O}_{7-\delta}$ ” (2024), arXiv:2402.10485.
- [22] H. Sakakibara, N. Kitamine, M. Ochi, and K. Kuroki, *Phys. Rev. Lett.* **132**, 106002 (2024).
- [23] D. Takegami, K. Fujinuma, R. Nakamura, M. Yoshimura, K.-D. Tsuei, G. Wang, N. N. Wang, J.-G. Cheng, Y. Uwatoko, and T. Mizokawa, *Phys. Rev. B* **109**, 125119 (2024).
- [24] T. Cui, S. Choi, T. Lin, C. Liu, G. Wang, N. Wang, S. Chen, H. Hong, D. Rong, Q. Wang, Q. Jin, J.-O. Wang, L. Gu, C. Ge, C. Wang, J.-G. Cheng, Q. Zhang, L. Si, K.-j. Jin, and E.-J. Guo, *Commun. Mat.* **5**, 32 (2024).
- [25] G. Heier, K. Park, and S. Y. Savrasov, *Phys. Rev. B* **109**, 104508 (2024).
- [26] W. Wú, Z. Luo, D.-X. Yao, and M. Wang, *Sci. China Phys. Mech. Astron.* **67**, 117402 (2024).
- [27] L. Craco and S. Leoni, *Phys. Rev. B* **109**, 165116 (2024).
- [28] H. Sakakibara, M. Ochi, H. Nagata, Y. Ueki, H. Sakurai, R. Matsumoto, K. Terashima, K. Hirose, H. Ohta, M. Kato, Y. Takano, and K. Kuroki, *Phys. Rev. B* **109**, 144511 (2024).
- [29] Z. Huo, Z. Luo, P. Zhang, A. Yang, Z. Liu, X. Tao, Z. Zhang, S. Guo, Q. Jiang, W. Chen, D.-X. Yao, D. Duan, and T. Cui, “Modulation of the octahedral structure and potential superconductivity of $\text{La}_3\text{Ni}_2\text{O}_7$ through strain engineering” (2024), arXiv:2404.11001.
- [30] M. Kakoi, T. Oi, Y. Ohshita, M. Yashima, K. Kuroki, T. Kato, H. Takahashi, S. Ishiwata, Y. Adachi, N. Hatada, T. Uda, and H. Mukuda, *J. Phys. Soc. Jpn.* **93**, 053702 (2024).
- [31] K. Jiao, R. Niu, H. Xu, W. Zhen, J. Wang, and C. Zhang, *Physica C* **621**, 1354504 (2024).
- [32] Y. Zhou, J. Guo, S. Cai, H. Sun, P. Wang, J. Zhao, J. Han, X. Chen, Y. Chen, Q. Wu, Y. Ding, T. Xiang, H. kwang Mao, and L. Sun, “Investigations of key issues on the reproducibility of high- T_c superconductivity emerging from compressed $\text{La}_3\text{Ni}_2\text{O}_7$ ” (2024), arXiv:2311.12361.
- [33] K. Chen, X. Liu, J. Jiao, M. Zou, C. Jiang, X. Li, Y. Luo, Q. Wu, N. Zhang, Y. Guo, and L. Shu, *Phys. Rev. Lett.* **132**, 256503 (2024).
- [34] F. Lechermann, S. Böttzel, and I. M. Eremin, *Phys. Rev. M* **8**, 074802 (2024).
- [35] B. Geisler, J. J. Hamlin, G. R. Stewart, R. G. Hennig, and P. J. Hirschfeld, *npj Quantum Mater.* **9**, 38 (2024).
- [36] Z. Liu, H. Sun, M. Huo, X. Ma, Y. Ji, E. Yi, L. Li, H. Liu, J. Yu, Z. Zhang, et al., *China Phys. Mech. Astron.* **66**, 217411 (2023).
- [37] P. Puphal, P. Reiss, N. Enderlein, Y.-M. Wu, G. Khalilullin, V. Sundaramurthy, T. Priessnitz, M. Knauft, L. Richter, M. Isobe, P. A. van Aken, H. Takagi, B. Keimer, Y. E. Suyolcu, B. Wehinger, P. Hansmann,

- and M. Hepting, “Unconventional crystal structure of the high-pressure superconductor $\text{La}_3\text{Ni}_2\text{O}_7$ ” (2023), arXiv:2312.07341.
- [38] H. Wang, L. Chen, A. Rutherford, H. Zhou, and W. Xie, *Inorg. Chem.* **63**, 5020 (2024).
- [39] L. Wang, Y. Li, S.-Y. Xie, F. Liu, H. Sun, C. Huang, Y. Gao, T. Nakagawa, B. Fu, B. Dong, Z. Cao, R. Yu, S. I. Kawaguchi, H. Kadobayashi, M. Wang, C. Jin, H.-k. Mao, and H. Liu, *J. Am. Chem. Soc.* **146**, 7506 (2024).
- [40] Y. Zhang, L.-F. Lin, A. Moreo, T. A. Maier, and E. Dagotto, *Nat. Commun.* **15**, 2470 (2024).
- [41] L. C. Rhodes and P. Wahl, *Phys. Rev. Mater.* **8**, 044801 (2024).
- [42] Y. Gu, C. Le, Z. Yang, X. Wu, and J. Hu, “Effective model and pairing tendency in bilayer ni-based superconductor $\text{La}_3\text{Ni}_2\text{O}_7$ ” (2023), arXiv:2306.07275.
- [43] J. Yang, H. Sun, X. Hu, Y. Xie, T. Miao, H. Luo, H. Chen, B. Liang, W. Zhu, G. Qu, C.-Q. Chen, M. Huo, Y. Huang, S. Zhang, F. Zhang, F. Yang, Z. Wang, Q. Peng, H. Mao, G. Liu, Z. Xu, T. Qian, D.-X. Yao, M. Wang, L. Zhao, and X. J. Zhou, *Nat Commun.* **15**, 4373 (2024).
- [44] D. A. Shilenco and I. V. Leonov, *Phys. Rev. B* **108**, 125105 (2023).
- [45] Z. Luo, X. Hu, M. Wang, W. Wú, and D.-X. Yao, *Phys. Rev. Lett.* **131**, 126001 (2023).
- [46] H. Yang, H. Oh, and Y.-H. Zhang, “Strong pairing from small fermi surface beyond weak coupling: Application to $\text{La}_3\text{Ni}_2\text{O}_7$ ” (2023), arXiv:2309.15095.
- [47] Y. Zhang, L.-F. Lin, A. Moreo, T. A. Maier, and E. Dagotto, *Phys. Rev. B* **108**, 165141 (2023).
- [48] Y.-F. Yang, G.-M. Zhang, and F.-C. Zhang, *Phys. Rev. B* **108**, L201108 (2023).
- [49] J. Chen, F. Yang, and W. Li, *Phys. Rev. B* **110**, L041111 (2024).
- [50] Y. Shen, M. Qin, and G.-M. Zhang, *Chinese Phys. Lett.* **40**, 127401 (2023).
- [51] V. Christiansson, F. Petocchi, and P. Werner, *Phys. Rev. Lett.* **131**, 206501 (2023).
- [52] H. Oh and Y.-H. Zhang, *Phys. Rev. B* **108**, 174511 (2023).
- [53] Y. Zhang, L.-F. Lin, A. Moreo, and E. Dagotto, *Phys. Rev. B* **108**, L180510 (2023).
- [54] Z. Liao, L. Chen, G. Duan, Y. Wang, C. Liu, R. Yu, and Q. Si, *Phys. Rev. B* **108**, 214522 (2023).
- [55] F. Lechermann, J. Gondolf, S. Böttzel, and I. M. Eremin, *Phys. Rev. B* **108**, L201121 (2023).
- [56] Y. Zhang, L.-F. Lin, A. Moreo, T. A. Maier, and E. Dagotto, *Phys. Rev. B* **109**, 045151 (2024).
- [57] T. Kaneko, H. Sakakibara, M. Ochi, and K. Kuroki, *Phys. Rev. B* **109**, 045154 (2024).
- [58] Y. Cao and Y.-f. Yang, *Phys. Rev. B* **109**, L081105 (2024).
- [59] H. LaBollita, V. Pardo, M. R. Norman, and A. S. Botana, “Electronic structure and magnetic properties of $\text{La}_3\text{Ni}_2\text{O}_7$ under pressure active role of the Ni- $d_{x^2-y^2}$ ” (2024), arXiv:2309.17279.
- [60] X. Chen, J. Choi, Z. Jiang, J. Mei, K. Jiang, J. Li, S. Agrestini, M. Garcia-Fernandez, X. Huang, H. Sun, D. Shen, M. Wang, J. Hu, Y. Lu, K.-J. Zhou, and D. Feng, “Electronic and magnetic excitations in $\text{La}_3\text{Ni}_2\text{O}_7$ ” (2024), arXiv:2401.12657.
- [61] Z. Ouyang, J.-M. Wang, J.-X. Wang, R.-Q. He, L. Huang, and Z.-Y. Lu, *Phys. Rev. B* **109**, 115114 (2024).
- [62] R. Jiang, J. Hou, Z. Fan, Z.-J. Lang, and W. Ku, *Phys. Rev. Lett.* **132**, 126503 (2024).
- [63] C. Lu, Z. Pan, F. Yang, and C. Wu, *Phys. Rev. Lett.* **132**, 146002 (2024).
- [64] B. Geisler, L. Fanfarillo, J. J. Hamlin, G. R. Stewart, R. G. Hennig, and P. J. Hirschfeld, “Optical properties and electronic correlations in $\text{La}_3\text{Ni}_2\text{O}_7$ bilayer nickelates under high pressure” (2024), arXiv:2401.04258.
- [65] Y.-H. Tian, Y. Chen, J.-M. Wang, R.-Q. He, and Z.-Y. Lu, *Phys. Rev. B* **109**, 165154 (2024).
- [66] C. C. Homes, S. V. Dordevic, D. A. Bonn, R. Liang, W. N. Hardy, and T. Timusk, *Phys. Rev. B* **71**, 184515 (2005).
- [67] S. Tajima, J. Schützmann, S. Miyamoto, I. Terasaki, Y. Sato, and R. Hauff, *Phys. Rev. B* **55**, 6051 (1997).
- [68] A. N. Lavrov, M. Y. Kameneva, and L. P. Kozeeva, *Phys. Rev. Lett.* **81**, 5636 (1998).
- [69] D. Mandrus, L. Forro, D. Koller, and L. Mihaly, *Nature* **351**, 460 (1991).
- [70] M. Dressel and G. Grüner, *Electrodynamics of solids: optical properties of electrons in matter* (Cambridge university press, 2002).
- [71] D. N. Basov and T. Timusk, *Rev. Mod. Phys.* **77**, 721 (2005).
- [72] S. J. Moon, C. C. Homes, A. Akrap, Z. J. Xu, J. S. Wen, Z. W. Lin, Q. Li, G. D. Gu, and D. N. Basov, *Phys. Rev. Lett.* **106**, 217001 (2011).
- [73] S. Uchida, K. Tamasaku, and S. Tajima, *Phys. Rev. B* **53**, 14558 (1996).
- [74] S. Uchida, T. Ido, H. Takagi, T. Arima, Y. Tokura, and S. Tajima, *Phys. Rev. B* **43**, 7942 (1991).
- [75] Z. G. Chen, T. Dong, R. H. Ruan, B. F. Hu, B. Cheng, W. Z. Hu, P. Zheng, Z. Fang, X. Dai, and N. L. Wang, *Phys. Rev. Lett.* **105**, 097003 (2010).
- [76] S. J. Moon, A. A. Schafgans, M. A. Tanatar, R. Prozorov, A. Thaler, P. C. Canfield, A. S. Sefat, D. Mandrus, and D. N. Basov, *Phys. Rev. Lett.* **110**, 097003 (2013).
- [77] B. Cheng, Z. G. Chen, C. L. Zhang, R. H. Ruan, T. Dong, B. F. Hu, W. T. Guo, S. S. Miao, P. Zheng, J. L. Luo, G. Xu, P. Dai, and N. L. Wang, *Phys. Rev. B* **83**, 144522 (2011).
- [78] T. Ishikawa, T. Kimura, T. Katsufuji, and Y. Tokura, *Phys. Rev. B* **57**, R8079 (1998).
- [79] B. Ruzicka, L. Degiorgi, H. Berger, R. Gaál, and L. Forró, *Phys. Rev. Lett.* **86**, 4136 (2001).
- [80] T. Katsufuji, M. Kasai, and Y. Tokura, *Phys. Rev. Lett.* **76**, 126 (1996).
- [81] N. E. Hussey, K. Nozawa, H. Takagi, S. Adachi, and K. Tanabe, *Phys. Rev. B* **56**, R11423 (1997).
- [82] A. Kaminski, S. Rosenkranz, H. M. Fretwell, Z. Z. Li, H. Raffy, M. Randeria, M. R. Norman, and J. C. Campuzano, *Phys. Rev. Lett.* **90**, 207003 (2003).
- [83] N. Kumar, T. P. Pareek, and A. M. Jayannavar, *Phys. Rev. B* **57**, 13399 (1998).
- [84] S. Chakravarty, A. Sudbø, P. W. Anderson, and S. Strong, *Science* **261**, 337 (1993).
- [85] C. C. Homes, T. Timusk, R. Liang, D. A. Bonn, and W. N. Hardy, *Phys. Rev. Lett.* **71**, 1645 (1993).
- [86] S. V. Dordevic, D. N. Basov, R. C. Dynes, and E. Bucher, *Phys. Rev. B* **64**, 161103 (2001).
- [87] Z. G. Chen, R. H. Yuan, T. Dong, and N. L. Wang, *Phys. Rev. B* **81**, 100502 (2010).
- [88] B. Su, Y. Song, Y. Hou, X. Chen, J. Zhao, Y. Ma, Y.

- Yang, J. Guo, J. Luo, and Z.-G. Chen, *Adv. Mater.* **31**, 1903498 (2019).
- [89] K. Takenaka, R. Shiozaki, S. Okuyama, J. Nohara, A. Osuka, Y. Takayanagi, and S. Sugai, *Phys. Rev. B* **65**, 092405.
- [90] A. A. Tsvetkov, J. Schützmann, J. I. Gorina, G. A. Kaljushnaia, and D. Van Der Marel, *Phys. Rev. B* **55**, 14152 (1997).
- [91] A. Ioffe and A. Regel, in *Progress in semiconductors* (1960) pp. 237–291.
- [92] N. F. Mott, *Philos Mag.* **26**, 1015 (1972).
- [93] N. E. Hussey, K. Takenaka, and H. Takagi, *Philos Mag.* **84**, 2847 (2004).
- [94] C. C. Homes, A. Akrap, J. S. Wen, Z. J. Xu, Z. W. Lin, Q. Li, and G. D. Gu, *Phys. Rev. B* **81**, 180508 (2010).
- [95] W. Z. Hu, J. Dong, G. Li, Z. Li, P. Zheng, G. F. Chen, J. L. Luo, and N. L. Wang, *Phys. Rev. Lett.* **101**, 257005 (2008).
- [96] J. Schützmann, S. Tajima, S. Miyamoto, and S. Tanaka, *Phys. Rev. Lett.* **73**, 174 (1994).
- [97] J. Schützmann, B. Gorshunov, K. F. Renk, J. Münzel, A. Zibold, H. P. Geserich, A. Erb, and G. Müller-Vogt, *Phys. Rev. B* **46**, 512 (1992).
- [98] C. Liu, G. D. Samolyuk, Y. Lee, N. Ni, T. Kondo, A. F. Santander-Syro, S. L. Bud'ko, J. L. McChesney, E. Rotenberg, T. Valla, A. V. Fedorov, P. C. Canfield, B. N. Harmon, and A. Kaminski, *Phys. Rev. Lett.* **101**, 177005 (2008).
- [99] C. Utfield, J. Laverock, T. D. Haynes, S. B. Dugdale, J. A. Duffy, M. W. Butchers, J. W. Taylor, S. R. Giblin, J. G. Analytis, J.-H. Chu, I. R. Fisher, M. Itou, and Y. Sakurai, *Physical Review B* **81**, 064509 (2010).
- [100] G. Wang, Y. Qian, G. Xu, X. Dai, and Z. Fang, *Phys. Rev. B* **104**, 047002 (2010).
- [101] A. Damascelli, Z. Hussain, and Z.-X. Shen, *Rev. Mod. Phys.* **75**, 473 (2003).
- [102] P. Giannozzi, S. Baroni, N. Bonini, M. Calandra, R. Car, C. Cavazzoni, D. Ceresoli, G. L. Chiarotti, M. Cococcioni, I. Dabo, A. Dal Corso, S. De Gironcoli, S. Fabris, G. Fratesi, R. Gebauer, U. Gerstmann, C. Gougousis, A. Kokalj, M. Lazzeri, L. MartinSamos, N. Marzari, F. Mauri, R. Mazzarello, S. Paolini, A. Pasquarello, L. Paulatto, C. Sbraccia, S. Scandolo, G. Sclauzero, A. P. Seitsonen, A. Smogunov, P. Umari, and R. M. Wentzcovitch, *J. Phys.: Condens. Matter* **21**, 395502 (2009).
- [103] G. Kresse and J. Furthmüller, *Phys. Rev. B* **54**, 11169 (1996).
- [104] J. P. Perdew, K. Burke, and M. Ernzerhof, *Phys. Rev. Lett.* **77**, 3865 (1996).
- [105] M. Van Setten, M. Giantomassi, E. Bousquet, M. Verstraete, D. Hamann, X. Gonze, and G.-M. Rignanese, *Compu. Phys. Commun.* **226**, 39 (2018).
- [106] S. L. Dudarev, G. A. Botton, S. Y. Savrasov, C. J. Humphreys, and A. P. Sutton, *Phys. Rev. B* **57**, 1505 (1998).
- [107] A. Kokalj, *Comput. Mater. Sci.* **28**, 155 (2003).
- [108] Y. Le Page and P. Saxe, *Phys. Rev. B* **65**, 104104 (2002).
- [109] X. Wu, D. Vanderbilt, and D. R. Hamann, *Phys. Rev. B* **72**, 035105 (2005).
- [110] A. Togo, L. Chaput, T. Tadano, and I. Tanaka, *J. Phys.: Condens. Matter* **35**, 353001 (2023).
- [111] A. Togo, *J. Phys. Soc. Jpn.* **92**, 012001 (2023).